

Anti-halo effects on reaction cross sections for $^{14,15,16}\text{C}$ isotopes

Takuma Matsumoto¹ and Masanobu Yahiro¹

¹*Department of Physics, Kyushu University, Fukuoka 812-8581, Japan*

(Dated: September 26, 2014)

We study anti-halo effects on reaction cross sections σ_R for $^{14,15,16}\text{C}$ scattering from a ^{12}C target at 83 MeV/nucleon, using the g -matrix double-folding model. ^{15}C is described by the $^{14}\text{C} + n$ two-body model that reproduces the measured large s -wave spectroscopic factor, i.e., the shell inversion that the $1s_{1/2}$ orbital is lower than the $0d_{5/2}$ orbital in energy. ^{16}C is described by the $^{14}\text{C} + n + n$ three-body model with the phenomenological three-body force (3BF) that explains the measured small s -wave spectroscopic factor. The 3BF allows the single-particle energies of the $^{14}\text{C} + n$ subsystem to depend on the position r of the second neutron from the center of mass of the subsystem. The $1s_{1/2}$ orbital is lower than the $0d_{5/2}$ orbital for large r , but the shell inversion is restored for small r . Anti-halo effects due to the “partial shell inversion” make σ_R for ^{16}C smaller than that for ^{15}C . We also investigate projectile breakup effects on the mass-number dependence of σ_R with the continuum discretized coupled-channels method.

PACS numbers: 21.45.-v, 24.10.Eq, 25.60.Dz, 25.60.Gc

I. INTRODUCTION

Unstable nuclei have exotic properties such as halo formation [1, 2] and shell evolution; see Ref. [3] for the recent review on shell evolution. Elucidation of these properties is an important subject in nuclear physics. Reaction cross section σ_R is a powerful experimental tool for determining matter radii of nuclei and hence searching for halo nuclei. In addition, theoretical analyses for σ_R are easier compared with other reactions. In fact, σ_R was measured recently for the scattering of Ne and Mg isotopes from a ^{12}C at 240 MeV/nucleon [4, 5], and the double-folding model (DFM) based on the Melbourne g -matrix [6] was successful in reproducing the data with no free parameter [7–10]. The analyses suggest that ^{31}Ne and ^{37}Mg are halo nuclei with large deformation.

Pairing correlations are known to be important for even nuclei. The correlation plays an important role particularly in weakly bound nuclei, since they are bound only with it. In the mean-field picture based on the Hartree-Fock Bogoliubov (HFB) method [11], the correlation makes quasi-particle energies deeper and then reduces the root-mean-square (RMS) radius of the matter density. This mechanism becomes significant for unstable nuclei where the separation energy is smaller than the gap energy. This suggests that the pairing correlation suppresses halo formation for even-even unstable nuclei. This is called the pairing anti-halo effect.

The pairing anti-halo effect is an interesting mechanism, but there is no clear evidence for the effect. Hagino and Sagawa suggested that the odd-even staggering in σ_R is possible evidence for the effect [12–14], using the HFB method for $^{30,31,32}\text{Ne} + ^{12}\text{C}$ scattering at 240 MeV/nucleon [4] and the few-body models for $^{14,15,16}\text{C} + ^{12}\text{C}$ scattering at 83 MeV/nucleon [15]. They introduced the parameter [14]

$$\gamma_3 = \sigma_R(A+1) - \frac{\sigma_R(A+2) + \sigma_R(A)}{2}, \quad (1)$$

where the mass number A of projectile is even in Eq. (1). The parameter γ_3 describes the deviation of $\sigma_R(A+1)$ for an odd

nucleus from the mean value $(\sigma_R(A+2) + \sigma_R(A))/2$ for even nuclei on both sides. Sasabe *et al.* extended their idea and defined the dimensionless odd-even deviation parameter [16]

$$\Gamma_R = \frac{\gamma_3}{[\sigma_R(A+2) - \sigma_R(A)]/2}, \quad (2)$$

where $\Gamma_R > 1$ when $\sigma_R(A+1) > \sigma_R(A+2)$. The parameter evaluated from measured σ_R has a large value of $\Gamma_R^{\text{exp}} = 2.0 \pm 0.8$ for $^{14,15,16}\text{C} + ^{12}\text{C}$ scattering at 83 MeV/nucleon [15]. The fact that $\Gamma_R^{\text{exp}} > 1$ shows that anti-halo effects play an important role in σ_R for ^{16}C . Sasabe *et al.* [16] analyzed the strong odd-even deviation with the continuum-discretized coupled-channels method (CDCC) [17–19] in order to take account of projectile breakup effects in addition to pairing (di-neutron) correlations. Here we identify di-neutron correlations with pairing ones. In the analysis, ^{15}C was described by the $^{14}\text{C} + n$ two-body orthogonality condition model (OCM) and ^{16}C was by the $^{14}\text{C} + n + n$ three-body OCM with the phenomenological three-body force (3BF) that reproduces the total binding energy. The theoretical calculations well reproduce σ_R for $^{14,15}\text{C}$, but the calculated odd-even deviation parameter is $\Gamma_R = 0.77$ and significantly undershoots $\Gamma_R^{\text{exp}} = 2.0 \pm 0.8$, although pairing correlations are taken into account in the three-body model. This implies that there exist other anti-halo effects besides the pairing anti-halo effect.

^{15}C is a halo nucleus with small one-neutron separation energy, $S_n = 1.218$ MeV. The s -wave spectroscopic factor λ_s in the ground state of ^{15}C is found to be $\lambda_s(^{15}\text{C}) = 0.97 \pm 0.08$ from Coulomb breakup measurements [20]. This means that the $1s_{1/2}$ orbital is lower than the $0d_{5/2}$ orbital in energy, i.e., the shell inversion takes place. The s -wave spectroscopic factor in the ground state of ^{16}C , meanwhile, is determined to be $\lambda_s(^{16}\text{C}) = 0.35 \pm 0.2$ from the measurements on longitudinal momentum distributions of ^{15}C fragments from ^{16}C breakup [21]. The suppression of λ_s from $\lambda_s(^{15}\text{C}) = 0.97 \pm 0.08$ to $\lambda_s(^{16}\text{C}) = 0.35 \pm 0.2$ is a key to clarifying the reason why Γ_R^{exp} is so large.

In this paper, we reanalyze $^{14,15,16}\text{C} + ^{12}\text{C}$ scattering at 83 MeV/nucleon by using the Melbourne g -matrix DFM and study the mechanism underlying the strong odd-even deviation.

tion of $\Gamma_R^{\text{exp}} = 2.0 \pm 0.8$. We introduce a surface-type 3BF to the $^{14}\text{C} + n + n$ three-body model to describe the suppression of λ_s from $\lambda_s(^{15}\text{C})$ to $\lambda_s(^{16}\text{C})$. The 3BF allows the single-particle energies of the $^{14}\text{C} + n$ subsystem to depend on the distance r between the second neutron and the center of mass of the $^{14}\text{C} + n$ subsystem. The $1s_{1/2}$ orbital is lower than the $0d_{5/2}$ orbital for large r , but the shell inversion is restored for small r . This is referred to as “partial shell inversion” in this paper. We show that the partial shell inversion enhances Γ_R largely. We also investigate projectile breakup effects on Γ_R with CDCC.

We briefly explain the DFM for nucleus–nucleus scattering and the few-body models for $^{15,16}\text{C}$ in Sec. II and show the results of model calculations in Sec. III. Section IV is devoted to summary.

II. MODEL SETTING

In the present g -matrix DFM, the optical potential U for nucleus–nucleus scattering is obtained by folding the Melbourne g -matrix with projectile and target densities; see Ref. [9] for the detail. The reaction cross section is obtained by solving the one-body Schrödinger with U for the elastic S -matrix elements. For a ^{12}C target, the matter density is assumed to be identical with the proton density deduced from the electron scattering [22], since the proton RMS radius deviates from the neutron one only by less than 1% in HFB calculations with the Gogny-D1S interaction [23]. For ^{14}C , the matter density is determined by HFB calculations, where the center-of-mass correction is made in the standard manner [9]. The matter radius of ^{14}C in the HFB calculation is $\bar{r}(^{14}\text{C}) = 2.51$ fm that is consistent with the measured charge radius 2.50 fm [24].

As for ^{15}C , we use the $^{14}\text{C} + n$ two-body OCM in which the Pauli-forbidden states are excluded in the modelspace [25]. The Hamiltonian is

$$h_2 = T_\rho + V_{nc}, \quad (3)$$

where T_ρ is the kinetic-energy operator with respect to the relative coordinate ρ between n and the core nucleus (^{14}C). The interaction V_{nc} between n and ^{14}C is taken from Ref. [12]. In this model, the shell inversion takes place, that is, the $1s_{1/2}$ orbital is lower than the $0d_{5/2}$ orbital. As a consequence of this property, this model well reproduces properties of the ground and 1st-excited states of ^{15}C such as $\lambda_s(^{15}\text{C}) = 0.97 \pm 0.08$. The matter radius of ^{15}C predicted by this model is $\bar{r}(^{15}\text{C}) = 2.87$ fm that is much larger than $\bar{r}(^{14}\text{C}) = 2.51$ fm. If the shell inversion does not take place, the calculated radius becomes $\bar{r}(^{15}\text{C}) = 2.65$ fm that is estimated by assuming the ground state with $0d_{5/2}$ and $S_n = 1.218$ MeV. The shell inversion is thus inevitable for ^{15}C to have a halo structure.

As for ^{16}C , we use the $^{14}\text{C} + n + n$ three-body OCM. The Hamiltonian is

$$h_3 = T_{\rho_1} + T_{r_1} + V, \quad (4)$$

which consists of the kinetic-energy operators T_{ρ_1} and T_{r_1} with respect to two Jacobi coordinates and the interaction V

defined by

$$V = V_{n_1 n_2} + V_{n_1 c} + V_{n_2 c} + V_3, \quad (5)$$

where $V_{n_1 n_2}$ is the two-nucleon force acting between two valence neutrons, n_1 and n_2 , and $V_{n_1 c}$ ($V_{n_2 c}$) is the interaction between n_1 (n_2) and ^{14}C . We use the Bonn-A two-nucleon force [26] as $V_{n_1 n_2}$ and the nucleon– ^{14}C interaction of Ref. [12] as $V_{n_1 c}$ and $V_{n_2 c}$. The interaction V_3 is the 3BF acting among n_1 , n_2 , and ^{14}C . We consider two types of 3BFs. One is a *volume-type 3BF* of

$$V_3^{(v)} = \sum_{c=1,2} V_0^{(v)} e^{-(\rho_c/\rho_0)^2} e^{-(r_c/r_0)^2}, \quad (6)$$

and the other is a *surface-type 3BF* of

$$V_3^{(s)} = \sum_{c=1,2} V_0^{(s)} \rho_c^2 e^{-(\rho_c/\rho_0)^2} e^{-(r_c/r_0)^2}, \quad (7)$$

where ρ_1 (ρ_2) is the coordinate of n_1 (n_2) from ^{14}C and r_1 (r_2) represents the coordinate of n_2 (n_1) from the center of mass of the n_1 (n_2) + ^{14}C subsystem. Assuming $\rho_0 = 0.76 \times 14^{1/3}$ fm and $r_0 = 2.54 \times 14^{1/3}$ fm, we determined $V_0^{(v)}$ and $V_0^{(s)}$ from the measured two-neutron separation energy $S_{2n}(\text{exp}) = 5.47$ MeV [27]; the resultant values are $V_0^{(v)} = -23.45$ MeV and $V_0^{(s)} = -6.18$ MeV/fm². Note that $T_{\rho_1} + T_{r_1} = T_{\rho_2} + T_{r_2}$ in Eq. (4).

For later convenience, we define the following four models by changing V : (I) $V = V_{n_1 c} + V_{n_2 c}$, (II) $V = V_{n_1 n_2} + V_{n_1 c} + V_{n_2 c}$, (III) $V = V_{n_1 n_2} + V_{n_1 c} + V_{n_2 c} + V_3^{(v)}$, and (IV) $V = V_{n_1 n_2} + V_{n_1 c} + V_{n_2 c} + V_3^{(s)}$. Using the four models, we calculate the probabilities P_s and P_d of $1s_{1/2}$ and $0d_{5/2}$ components in the ground state of ^{16}C , the matter radius $\bar{r}(^{16}\text{C})$, and S_{2n} . The probabilities are obtained by taking the overlap between the ground state of ^{16}C and the $1s_{1/2}$ and $0d_{5/2}$ states of ^{15}C . The difference between models II and III (IV) shows effects of the volume-type (surface-type) 3BF, whereas the difference between models I and II describes effects of pairing correlations.

In actual calculations, we used the Gaussian expansion method [28] in which h_2 and h_3 are diagonalized in a space spanned by Gaussian basis functions with geometric progression range parameters.

III. RESULTS

A. Ground-state properties of ^{16}C

Table I shows a comparison of four models for P_s , P_d , the ratio $\delta = \bar{r}(^{16}\text{C})/\bar{r}(^{15}\text{C})$, and S_{2n} . In model I, P_s is almost 100%, so that ^{16}C has a halo structure of $\delta = 1.09$. In model II where V_{nn} is added to model I, P_s decreases to 79% whereas P_d increases to 16%, so that δ is reduced to 1.04. Thus pairing correlations surely reduce δ , but the reduction is only 5%. The value of S_{2n} for model II is still smaller than the experimental value $S_{2n}(\text{exp}) = 5.47$ MeV. This indicates that the

introduction of phenomenological 3BF is necessary. In model III where $V_3^{(v)}$ is added to model II, P_s and P_d are close to the results in model II. The reduction of δ due to $V_3^{(v)}$ is 6% and comparable with that due to pairing correlation. In model IV where $V_3^{(s)}$ is added to model II, however, P_s is largely reduced to 15% that is consistent with the measured value $\lambda_s(^{16}\text{C}) = 0.35 \pm 0.2$, so that δ is reduced from 1.04 to 0.95. The reduction of δ due to $V_3^{(s)}$ is thus 9% and twice as much as that due to pairing correlation.

TABLE I: Comparison of four models for the probabilities P_s , P_d of $1s_{1/2}$ and $0d_{5/2}$ components in the ground state of ^{16}C , the ratio $\delta = \bar{r}(^{16}\text{C})/\bar{r}(^{15}\text{C})$ and the two-neutron separation energy S_{2n} , and the odd-even deviation parameter Γ_{rds} .

Models	P_s [%]	P_d [%]	δ	S_{2n} [MeV]	Γ_{rds}
I	99	0	1.09	2.40	0.11
II	79	16	1.04	3.22	0.52
III	72	14	0.98	5.47	1.50
IV	15	74	0.95	5.47	2.48

We make the following analysis to study the mechanism underlying the large reduction of P_s due to $V_3^{(s)}$. We start with the approximate Hamiltonian $T_{\rho_1} + V_{n_1c}(\rho_1)$ instead of h_3 . For the approximate Hamiltonian, one can clearly define the single-particle energies in the $^{14}\text{C} + n$ subsystem of ^{16}C . The effects of 3BF on the single-particle energies can be estimated by adding a half of 3BF to the approximate Hamiltonian:

$$h'_3(r_1) = T_{\rho_1} + V_{n_1c}(\rho_1) + V_3(\rho_1, r_1), \quad (8)$$

where $V_3(\rho_1, r_1)$ is the $c = 1$ part of V_3 and the OCM is taken. The single-particle energies of $h'_3(r_1)$ are obtained as a function of r_1 . The single-particle energies are plotted as a function of r for $1s_{1/2}$ and $0d_{5/2}$ orbitals in Fig. 1, where we have used r as the shorthand notation of r_1 . In panel (a) for the volume-type 3BF, the $1s_{1/2}$ orbital is lower than the $0d_{5/2}$ orbital for any r . The shell inversion thus takes place for any r . In panel (b) for the surface-type 3BF, meanwhile, the $1s_{1/2}$ orbital is lower than the $0d_{5/2}$ orbital at large r , but the shell inversion is restored at $r < 5$ fm. This partial shell inversion is an origin of the large reduction of P_s due to $V_3^{(s)}$.

Now we consider the sum $\bar{R}(A) = \bar{r}(A) + \bar{r}(A_T)$ of projectile and target RMS radii $\bar{r}(A)$ and $\bar{r}(A_T)$, and introduce the dimensionless odd-even deviation parameter Γ_{rds} for $\bar{R}(A)$ as

$$\Gamma_{\text{rds}} = \frac{\bar{R}^2(A+1) - [\bar{R}^2(A) + \bar{R}^2(A+2)]/2}{[\bar{R}^2(A+2) - \bar{R}^2(A)]/2}, \quad (9)$$

where the mass number A_T of target is 12 in the present case. The parameter Γ_{rds} has the same property as Γ_R ; namely, $\Gamma_{\text{rds}} > 1$ when $\bar{R}(A+1) > \bar{R}(A+2)$.

The parameter Γ_{rds} is also tabulated in Table I for four models. In model I, Γ_{rds} is much smaller than 1. In model II where $V_{n_1n_2}$ is added to model I, Γ_{rds} becomes slightly large but still smaller than 1. Comparing models III and IV with model II, one can see that the enhancement of Γ_{rds} due to $V_3^{(v)}$ is much

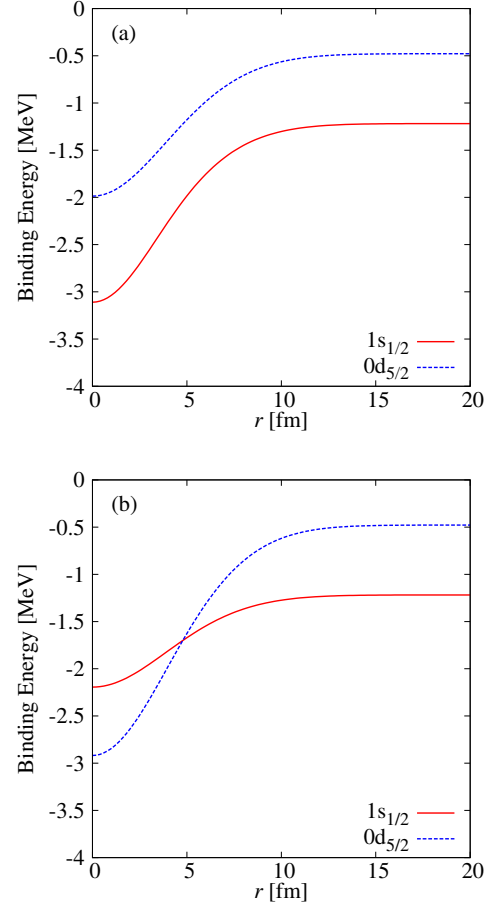


FIG. 1: (Color online) r dependence of single particle energies in the $^{14}\text{C} + n$ subsystem of ^{16}C . Panels (a) and (b) correspond to the results of the volume- and surface-type 3BFs, respectively. The solid (dashed) line corresponds to the $1s_{1/2}$ ($0d_{5/2}$) orbital.

larger than that due to $V_{n_1n_2}$ and the enhancement of Γ_{rds} due to $V_3^{(s)}$ is even larger than that due to $V_3^{(v)}$. The partial shell inversion is thus important as an origin of the odd-even deviation in $\bar{R}(A)$, and Γ_{rds} is a good quantity to detect the partial shell inversion.

B. Reaction cross sections

The parameter Γ_R is identical with Γ_{rds} , if the following two conditions are satisfied. The first condition is that projectile breakup is negligible. If it is significant, the effects on σ_R are larger for ^{15}C projectile than for ^{16}C projectile, since ^{15}C has much smaller S_n than ^{16}C . This enhances Γ_R from Γ_{rds} , but the following second condition is more significant in the present case. For simplicity, let us assume that projectile breakup is negligible. When the absolute value of the elastic S -matrix element is 0 for orbital angular momenta L corresponding to the nuclear interior and 1 for L to the nuclear exterior, it is satisfied that $\sigma_R(A) = \pi \bar{R}^2(A)$. This situation

is called the black-sphere scattering (BSS). Hence Γ_R agrees with Γ_{rds} , when the BSS is realized and projectile breakup is negligible. The present scattering largely differs from the BSS [16], so that Γ_R is much reduced from Γ_{rds} by the non-BSS effect, as shown below.

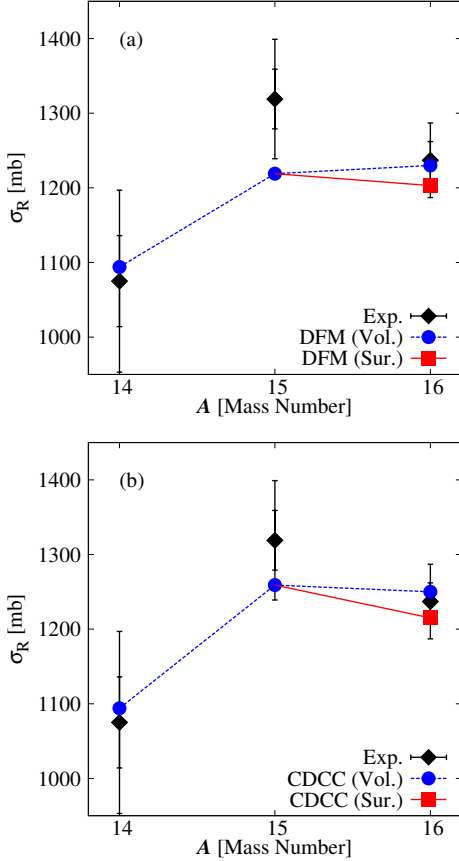


FIG. 2: (Color online) Reaction cross sections σ_R for $^{14,15,16}\text{C} + ^{12}\text{C}$ scattering at 83 MeV/nucleon. Panels (a) and (b) represent the results of DFM and CDCC calculations, respectively. For $^{14,15}\text{C}$, the circles show the results of theoretical calculations. For ^{16}C , the circle and square correspond to the results of the volume-type and surface-type 3BFs, respectively. The experimental data are taken from Ref. [15] and are plotted with $2\text{-}\sigma$ error (95.4% certainty).

It is not easy to estimate projectile breakup effects when the coupling potentials among elastic and breakup channels are calculated within the framework of the g -matrix double folding, since it requires time-consuming calculations. We then do CDCC calculations by assuming the $^{14}\text{C} + n + ^{12}\text{C}$ three-body model for $^{15}\text{C} + ^{12}\text{C}$ scattering and the $^{14}\text{C} + n + n + ^{12}\text{C}$ four-body model for $^{16}\text{C} + ^{12}\text{C}$ scattering. The optical potentials U_x between $x (= n, ^{14}\text{C})$ and a ^{12}C target are constructed by folding the Melbourne g -matrix with densities of x and ^{12}C . The optical potential U_n is slightly reduced so that the single-channel calculation with no projectile breakup can yield the same σ_R as the DFM. The detail of CDCC calculations is the same as in Ref. [16]. Coulomb breakup is neglected, since it is small. Convergence of CDCC solutions with respect to increasing the modelspace is confirmed for σ_R .

Figure 2 shows σ_R for $^{14,15,16}\text{C} + ^{12}\text{C}$ scattering at 83 MeV/nucleon. The parameter Γ_R is tabulated in Table II for models III and IV. In panel (a) of Fig. 2, the results of the DFM are plotted as a function of A . For $^{14,15}\text{C}$, the theoretical results are shown by circles. For ^{16}C , the theoretical results are plotted by a circle for the volume-type 3BF and by a square for the surface-type 3BF. The parameter Γ_R is 1.24 and larger than 1 for the surface-type 3BF, whereas $\Gamma_R = 0.79$ for the volume-type 3BF. The reaction cross sections thus have strong odd-even deviation for the surface-type 3BF. The reduction from $\Gamma_{\text{rds}} = 2.48$ to $\Gamma_R = 1.24$ for the surface-type 3BF is due to the non-BBS effect. In panel (b), projectile breakup corrections are added to the results of panel (a). The results well reproduce the measured σ_R for $^{14,15,16}\text{C}$ [15]; here the data are plotted with $2\text{-}\sigma$ error (95.4% certainty). Projectile breakup enhances Γ_R from 1.24 to 1.78 for the surface-type 3BF and from 0.79 to 1.12 for the volume-type 3BF. The difference between $\Gamma_R = 1.78$ and 1.12 comes from presence or absence of the partial shell inversion. Both the partial shell inversion and the projectile breakup effect are thus important for the surface-type 3BF. The final result $\Gamma_R = 1.78$ with the partial shell inversion and the projectile breakup effect is consistent with the experimental value $\Gamma_R^{\text{exp}} = 2.0 \pm 0.8$.

TABLE II: Summary of odd-even deviation parameters Γ_R .

Models	$\Gamma_R(\text{DFM})$	$\Gamma_R(\text{CDCC})$	Γ_R^{exp}
III	0.79	1.12	2.0 ± 0.8
IV	1.24	1.78	

IV. SUMMARY

we reanalyzed $^{14,15,16}\text{C}$ scattering from a ^{12}C target at 83 MeV/nucleon with the Melbourne g -matrix DFM and studied the mechanism underlying the strong odd-even deviation of $\Gamma_R^{\text{exp}} = 2.0 \pm 0.8$. We introduced a surface-type 3BF to the $^{14}\text{C} + n + n$ three-body model in order to describe the suppression of the s-wave spectroscopic factor from $\lambda_s(^{15}\text{C}) = 0.97 \pm 0.08$ to $\lambda_s(^{16}\text{C}) = 0.35 \pm 0.2$. The 3BF allows the single-particle energies of the $^{14}\text{C} + n$ subsystem to depend on the position r of the second neutron from the center of mass of the $^{14}\text{C} + n$ subsystem. The $1s_{1/2}$ orbital is lower than the $0d_{5/2}$ orbital for large r , but the shell inversion is restored for small r . The suppression of $\lambda_s(^{16}\text{C})$ due to the partial shell inversion is stronger than that due to pairing correlation. Also for $\bar{r}(^{16}\text{C})$, Γ_{rds} and Γ_R , anti-halo effects due to the partial shell inversion are more important than the pairing anti-halo effect and make the matter radius of ^{16}C smaller than that of ^{15}C and eventually enhances Γ_R largely. CDCC calculations with effects of projectile breakup and the partial shell inversion yield $\Gamma_R = 1.72$ that is consistent with the experimental value $\Gamma_R^{\text{exp}} = 2.0 \pm 0.8$. We therefore conclude that both the partial shell inversion and the projectile breakup effect in addition to pairing (di-neutron) correlations are important to describe the strong odd-even deviation of $\Gamma_R^{\text{exp}} = 2.0 \pm 0.8$.

The parameter Γ_R^{exp} is also large for $^{30,31,32}\text{Ne} + ^{12}\text{C}$ scattering at 240 MeV/nucleon [4]. Projectile breakup effects are small because of the high incident energy [8]. Meanwhile, the shell inversion may take place also in ^{31}Ne [8]. This suggests that the partial shell inversion takes place also for ^{31}Ne . If reaction cross sections are measured systematically at higher incident energies such as 240 MeV/nucleon, the Γ_R determined from the measurement may detect presence or absence of the partial shell inversion. Systematic measurements of Γ_R and accurate theoretical analyses of measured Γ_R are quite inter-

esting as a future work.

Acknowledgments

The authors would like to thank Fukuda and Yamaguchi for helpful discussions. M. Y. is supported by Grant-in-Aid for Scientific Research (No. 26400278) from the Japan Society for the Promotion of Science (JSPS).

-
- [1] I. Tanihata *et al.*, Phys. Rev. Lett. **55**, 2676 (1985); Phys. Lett. **B206**, 592 (1988). I. Tanihata, J. Phys. G **22**, 157 (1996).
 - [2] A. Ozawa *et al.*, Nucl. Phys. **A691**, 599 (2001).
 - [3] O. Sorlin, EPJ Web Conf. **66**, 01016 (2014) [arXiv:1401.1378 [nucl-ex]].
 - [4] M. Takechi *et al.*, Phys. Lett. **B707**, 357 (2012).
 - [5] M. Takechi *et al.*, submitted to Phys. Rev. Lett., EPJ Web of Conferences **66**, 02101 (2014).
 - [6] K. Amos *et al.*, in *Advances in Nuclear Physics*, edited by J. W. Negele and E. Vogt (Plenum, New York, 2000) Vol. 25, p. 275.
 - [7] K. Minomo *et al.*, Phys. Rev. C **84**, 034602 (2011).
 - [8] K. Minomo *et al.*, Phys. Rev. Lett. **108**, 052503 (2012).
 - [9] T. Sumi *et al.*, Phys. Rev. C **85**, 064613 (2012).
 - [10] S. Watanabe *et al.*, Phys. Rev. C **89**, 044610 (2014).
 - [11] K. Bennaceur *et al.*, Phys. Lett. **B496**, 154 (2000).
 - [12] K. Hagino and H. Sagawa, Phys. Rev. C **84**, 011303 (2011).
 - [13] K. Hagino and H. Sagawa, Phys. Rev. C **85**, 014303 (2012).
 - [14] K. Hagino and H. Sagawa, Phys. Rev. C **85**, 037604 (2012).
 - [15] D.Q. Fang *et al.*, Phys. Rev. C **69**, 034613 (2004).
 - [16] S. Sasabe *et al.*, Phys. Rev. C **88**, no. 3, 037602 (2013).
 - [17] M. Kamimura *et al.*, Prog. Theor. Phys. Suppl. **89**, 1 (1986).
 - [18] N. Austern *et al.*, Phys. Rep. **154**, 125 (1987).
 - [19] M. Yahiro *et al.*, Prog. Theor. Exp. Phys. 2012, 01A206 (2012).
 - [20] U. Datta Pramanik *et al.*, Phys. Lett. B **351**, 63 (2003).
 - [21] T. Yamaguchi *et al.*, Nucl. Phys. A **724**, 3 (2003).
 - [22] H. de Vries *et al.*, At. Data Nucl. Data Tables **36**, 495 (1987).
 - [23] J. F. Berger *et al.*, Comput. Phys. Commun. **63**, 365 (1991).
 - [24] L.A. Schaller *et al.*, Nucl. Phys. **A379**, 523 (1982).
 - [25] S. Saito, Prog. Theor. Phys. **41**, 705 (1969).
 - [26] R. Machleidt, Adv. Nucl. Phys. **19**, 189 (1989).
 - [27] D. R. Tilley *et al.*, Nucl. Phys. **A565**, 1 (1993).
 - [28] E. Hiyama *et al.*, Prog. Part. Nucl. Phys. **51**, 223 (2003).